Geophys. J. R. astr. Soc. (1978) **55**, 471–497

The evolution of sedimentary basins on a viscoelastic lithosphere: theory and examples

Christopher Beaumont *Oceanography Department, Dalhousie University, Halifax, Nova Scotia, Canada B3H 3J5*

Received 1978 April 24; in original form 1978 March 7

Summary. A systematic approach is suggested for modelling the development of sedimentary basins. The theory, which partitions basin formation into initiating and isostatic adjustment processes, is applicable to all modes of basin formation if these processes are linear, or can be represented with sufficient accuracy in an incrementally linear form.

The dynamics of regional isostatic adjustment are characterized by the Heaviside space-time Green functions for the response of elastic and viscoelastic (Maxwell) thin plate models of the lithosphere. It is shown, by convolving the Heaviside–Green functions with cylindrical surface loads, that the rate of isostatic adjustment on a viscoelastic lithosphere is a function of the wavelength of the surface load, long wavelengths being compensated most rapidly.

Six archetypal initiating processes for sedimentary basin development are presented. These processes are those responsible for the subsidence of the Earth's surface which creates a depression in which water and sediments collect. Isostatic amplification of subsidence by sediment and water loads is cast in the form of an integral equation with isostatic Heaviside–Green functions as kernel.

Specific examples, the basins that result from a graben initiating process, are compared with the largest scale structure of the North Sea Basin, a basin that is known to be underlain by a graben system. A model, in which a 50-km wide graben subsides exponentially with a time constant of 5×10^7 yr during the interval 180–100 Myr BP, is shown to be consistent with the largest scale structure of the North Sea Basin if the underlying lithosphere is viscoelastic with a flexural rigidity of $\sim 5 \times 10^{25}$ Nm and relaxation time constant $\sim 10^6$ yr.

1 Introduction

There is no doubt that the plate tectonic model of geodynamics explains most of the significant geological features of the Earth's surface that can be attributed to the horizontal

interactions of plates at their boundaries. However, the theory for long-term vertical movements is not so well developed. Undoubtedly, vertical movements are intimately coupled to their horizontal counterparts, but because of their smaller magnitude they have not received as much attention. The only generally agreed-upon principles for interpreting vertical movements are those of isostasy, and thermal expansion associated with conductive heat transfer. Although these principles lead to physically reasonable models that match ocean bathymetry and the subsidence of some continental margins, there is still no agreement on the rheological properties of the lithosphere or asthenosphere, and consequently on the dynamics of isostasy. It is also clear that the simple thermal models provide only an incomplete description of long-term vertical motions in the continental interiors (Sleep & Snell 1976).

The purpose of this paper is to suggest that the best record of vertical movements over time-scales of 10^7 to 10^8 yr is stored in the stratigraphy of sedimentary basins, and to propose a class of models describing the dynamics of sedimentary basin formation where the underlying lithosphere is either elastic or viscoelastic (a Maxwell body). (The term viscoelastic is used in this paper for the Maxwell rheology in the common usage sense that all rheologies that can be represented by series–parallel combinations of the spring and dashpot force extension model are viscoelastic. Strictly speaking, the Maxwell body is a fluid and is therefore elasticoviscous.) The model requires a knowledge, or a hypothetical description, of either the forces responsible for initiating vertical movements or the resulting topographic change. Having specified these, the forward calculation predicts the subsidence and sediment accumulation within the basin with time. The results can be compared with stratigraphy of well cores and with sections based on seismic reflection profiles.

Ideally, a complete description of a basin's age–depth stratigraphy that has been corrected for movements within the sediment column (e.g. halokinesis) is needed for comparison with model predictions. In practice, the observations are imperfect and some judgement is always involved in deciding whether the subsidence recorded in the stratigraphy is true basement subsidence. Basins with little salt or shale are obviously preferable. The palaeobathymetry of the basin is the remaining major problem in deducing the amount of subsidence. Sediments deposited in a deltaic or nearshore environment will have subsided by almost their present depth if the sea-level has remained constant. It is, however, difficult to quantify palaeobathymetry on the basis of an outer neritic or bathyal environment. Variations in palaeobathymetry do not invalidate the proposed model because transgressions, regressions and basin starvation can easily be included. Such variations do, however, introduce additional variables and the model loses its simplicity and ability to be definitive, unless the times at which the eustatic sea-level changes, etc., occurred are known.

The proposed basin model has two essential components; the initiating mechanism, which creates a depression in which sediments can collect, and an ability to model the dynamics of regional isostatic adjustment under the sedimentary load. The first half of the paper is devoted to a description of the latter component, the rheology of the lithosphere and the dynamics of isostatic adjustment. This is followed by a short description of kinematic models that may describe initiating mechanisms. The paper is completed with an example, that of a graben initiated basin, and a comparison of the model results with the North Sea sedimentary basin.

2 Rheology of the lithosphere

The rationale for modelling the development of sedimentary basins on both elastic and viscoelastic lithospheres is to try to determine which, if either, of these two models is

correct. Other possible rheologies are, for example, power-law creep (Murrell 1976) or perfect plasticity (Turcotte, McAdoo & Caldwell 1978). The most complicated rheology employed in this paper is linear viscoelasticity. Success, or failure, of the resulting models determines the need for a more complex and non-linear theology.

The main parameters that characterize the deformation of a thin viscoelastic lithosphere overlying an inviscid asthenosphere, assuming thin plate theory, are the flexural rigidity, D, and the relaxation time constant, τ (see the section on the response of elastic and viscoelastic lithosphere to a Heaviside point load and Fig. 2). Walcott (1970) plotted the change in apparent flexural rigidity (the best-fitting flexural rigidity assuming an elastic lithosphere) as a function of age of the topographic load. His graph is reproduced in Fig. 1 with additional results from studies noted in the figure caption. The seismic estimate of the flexural rigidity is also added to emphasize that there is no conflict between the rheological and seismological concepts of the lithosphere if the lithosphere is capable of viscous relaxation.

That the flexural rigidity does indeed decrease with age of the topographic load indicates that the lithosphere is at least viscoelastic. No firm conclusion on the form of the relaxation or the existence of a yield strength can be made from Fig. 1 because the individual loads act on different areas of the lithosphere and the properties of the lithosphere are known to vary with age and location. Moreover, and probably of greater import, the areal distribution of the load has been ignored in many cases. It is shown in a later section that this leads to incorrect results because the rate of isostatic adjustment on a viscoelastic lithosphere is citically dependent on the wavelength of the load. Despite these problems, initial trial values

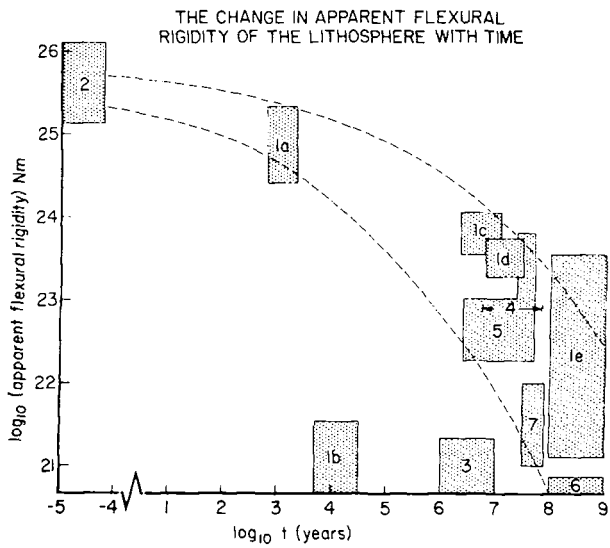

Figure 1. Apparent flexural rigidity as a function of age of the surface load. The apparent flexural rigidity is the flexural rigidity of the elastic plate that most closely agrees with the observations. The results 1(a–e) are from Walcott (1970) and were derived from the following areas: 1a Lake Agassiz and Lake Algonquin, 1b Lake Bonneville, 1c the Interior Plains and Caribou Mountains, 1d Hawaiian Archipelago and Island Arcs, 1e the Boothia Uplift. 2 is the seismic estimate explained in the text. 3 is from the Kuril Trench–Hokkaido Rise system (Hanks 1971). 4 is from the Great Meteor seamount (Watts *et al.* 1975). 5 is from the Hawaiian–Emperor seamount chain (Watts & Cochran 1974). 6 is from topography and gravity in Australia (McNutt & Parker 1977). 7 is from topography and gravity from the continental United States (Banks *et al.* 1977). (Note: it is not really valid to consider 1(a) and (b) in this context because they measure asthenospheric flow.)

of the parameters D (10^{25}–10^{26} Nm) and τ (10^5–10^6 yr) for the basin calculation can be inferred from Fig. 1. Deviations from these values by more than an order of magnitude would be inconsistent with the observations. This result is based on the argument that the seismological and rheological definitions of the lithosphere are the same if the lithosphere is viscoelastic.

The value of D is best estimated from seismological results. If average values of $2 \times 10^{11}\,\mathrm{Nm^{-2}}$ and 0.25 are assumed for Young's modulus (E) and Poisson's ratio (σ), then $D = Ed^3/12(1-\sigma^2) = 1.42 \times 10^{26}$ Nm for a lithosphere of thickness (d) = 200 km. Similarly, $D = 1.78 \times 10^{25}$ Nm for a lithosphere of thickness 100 km. Consequently, $D = 10^{25}$ Nm for older oceanic lithosphere and $D = 10^{26}$ Nm for continental lithosphere are appropriate trial values. If the seismological and rheological concepts of the lithosphere prove irreconcilable, a greater range of values of D and τ must be explored.

3 The response of elastic and viscoelastic lithospheres to a Heaviside point load

3.1 THE MODEL

The model considered here (Fig. 2) comprises a thin elastic or viscoelastic plate overlying an inviscid fluid asthenosphere. Two rationalizations are required to justify the simplicity of the model. The first is linear rheology, discussed in the introduction; the second is an inviscid asthenosphere. Peltier (1974) has considered the more complete problem of the response of a self-gravitating spherical Maxwell earth to applied surface loads for time-scales up to 2×10^4 yr. His results, and observational evidence from glacial rebound (Cathles 1975; Peltier & Andrews 1976; Walcott 1973), indicate a characteristic relaxation time for the asthenosphere on deglaciation of a few thousand years (corresponding to a viscosity of $\sim 10^{22}$ poise). This relaxation time is two orders of magnitude smaller than the lowest value proposed for the lithosphere. It is therefore reasonable to assume as a first approximation that the asthenosphere is an inviscid fluid when modelling the formation of sedimentary basins over time-scales of 10^7 to 10^8 yr. The simplicity of the two-parameter earth model can also be justified because our knowledge of sedimentary basin formation is primitive by comparison with that of isostatic rebound following the Wisconsin deglaciation.

The deformation of a thin elastic or viscoelastic plate overlying an inviscid fluid substratum has been studied by Hertz (1884); Gunn (1943); Jeffreys (1959); Nadai (1963, chapter 10) and Walcott (1970) among others. Their results are inappropriate for this discussion because they are either two-dimensional, assuming a line surface load, or do not

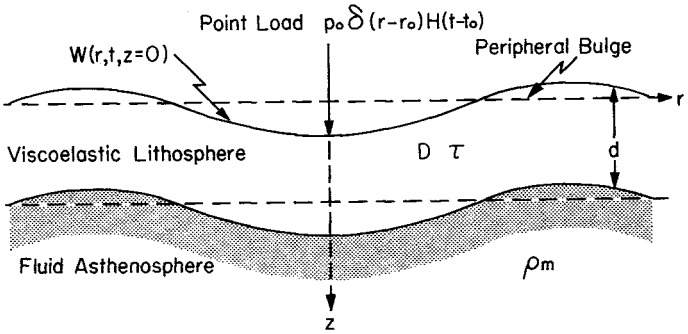

Figure 2. Section through the thin plate model of the lithosphere. See text for an explanation of the symbols.

follow a Green function–convolution integral approach that is central to the development of this paper. An integral transform method is developed here to describe the response of both elastic and viscoelastic plates under a point load that is applied at $t = 0$.

3.2 THE ELASTIC PLATE

The equation describing the vertical deflection $w(r)$ of an elastic plate overlying a fluid substratum is (Nadai 1963, p. 261)

$$D\nabla^4 w(r) + \gamma_s w(r) = p(r), \tag{1}$$

where $\gamma_s = (\rho_m - \rho_s)g$. g is the acceleration due to gravity, ρ_m is the density of the substratum (asthenosphere) and ρ_s is the density of the sediments or water that may fill the depression.

D = the flexural rigidity = $Ed^3/12(1 - \sigma^2)$

where E and σ are the Young's modulus and Poisson's ratio of the plate and d its thickness. $p(r)$ is the applied surface load. Taking the zeroth-order Hankel transform on the r variable, where

$$\bar{f}(\xi) = \int_0^\infty f(r) J_0(\xi r) r dr$$

and

$$f(r) = \int_0^\infty \bar{f}(\xi) J_0(\xi r) \xi d\xi$$

are the Hankel transform pair, yields

$$D\xi^4 \bar{w}(\xi) + \gamma_s \bar{w}(\xi) = \bar{p}(\xi).$$

Define the flexural parameter $\alpha = (4D/\gamma_s)^{1/4}$ and substitute for γ_s; then

$$\bar{w}(\xi) = \frac{\bar{p}(\xi)}{D}\left[\frac{1}{\xi^4 + 4/\alpha^4}\right].$$

If $p(r)$ is explicitly taken to be $p_0\delta(r)$, then $\bar{p}(\xi) = -p_0/2\pi$ (Sneddon 1951, p. 471). Therefore,

$$w(r) = G^E(r - r_0) = \frac{-p_0}{2\pi D}\int_0^\infty \left[\frac{1}{\xi^4 + 4/\alpha^4}\right] J_0(\xi r)\xi d\xi.$$

From standard tables of Hankel transforms (e.g. Oberhettinger 1972)

$$G^E(r - r_0) = \frac{-p_0}{\pi\alpha^2\gamma_s} Kei_0\left(\frac{\sqrt{2}r}{\alpha}\right) \tag{2}$$

where Kei_0 is the zeroth-order Kelvin function Kei, and $G^E(r - r_0)$ is the Green function for the elastic plate.

This solution is equivalent to the more cumbersome integral expression

$$G^E(r - r_0) = \frac{-p_0}{\pi\alpha^2\gamma_s}\int_1^\infty \frac{\exp(-rv/\alpha)}{(v^2 - 1)^{1/2}} \sin\left(\frac{rv}{\alpha}\right) dv$$

given by Hertz (1884) and used by Walcott (1970) and Watts, Cochran & Selzer (1975). The expression used by these authors is in error by a factor of ½ which results in an underestimate of the flexural parameter and flexural rigidity by $\sqrt{2}$ and 4 respectively.

3.3 THE VISCOELASTIC PLATE

The equation describing the deformation $w(r, t)$ of a thin viscoelastic plate overlying an inviscid fluid is

$$D\nabla^4 \dot{w}(r, t) + \gamma_s\left(\dot{w}(r, t) + \frac{w(r, t)}{\tau}\right) = \dot{p}(r, t) + \frac{p(r, t)}{\tau}. \tag{3}$$

This is equivalent to Nadai's equation 10.3, p. 285 (for the bending of a two-dimensional beam) and assumes that the plate is elastically incompressible, Poisson's ratio = 0.5. The dot denotes differentiation with respect to time and τ is the relaxation time, a measure of the viscosity of the plate. Other parameters are the same as those for the elastic plate, equation (1). If a cylindrically symmetric load function and cylindrical coordinates are chosen, the equation can be solved by taking the zeroth-order Hankel transform on the r variable and the Laplace transform on the t variable. The Hankel transformed equation is

$$D\xi^4 \frac{\partial \bar{w}}{\partial t}(\xi, t) + \gamma_s\left(\frac{\partial \bar{w}}{\partial t}(\xi, t) + \frac{\bar{w}}{\tau}(\xi, t)\right) = \frac{\partial \bar{p}}{\partial t}(\xi, t) + \frac{\bar{p}}{\tau}(\xi, t). \tag{4}$$

For the present take $p(r, t) = p'(r)H(t - t_0)$, that is, leave the spatial dependence undefined, but take the time dependence as a Heaviside step applied at $t = t_0$. Consequently, $\dot{p}(r, t) = p'(r)\delta(t - t_0)$ and $\partial\bar{p}(\xi, t)/\partial t = \bar{p}'(\xi)\delta(t - t_0)$. Substituting in (4) gives

$$D\xi^4 \frac{\partial \bar{w}}{\partial t}(\xi, t) + \gamma_s\left(\frac{\partial \bar{w}}{\partial t}(\xi, t) + \frac{\bar{w}}{\tau}(\xi, t)\right) = \bar{p}'(\xi)\delta(t - t_0) + \frac{\bar{p}'}{\tau}(\xi)H(t - t_0). \tag{5}$$

Take the Laplace transform of (5), where

$$\mathscr{L}[F(t)] = f(s) = \int_0^\infty \exp(-st)F(t)\,dt$$

and

$$F(t) = \frac{1}{2\pi i}\oint_c \exp(st)f(s)\,ds, \quad t > 0$$

define the Laplace transform pair, and c is the Bromwich path,

$$(D\xi^4 + \gamma_s)(sW(\xi, s) - \bar{w}(\xi, 0)) + \frac{\gamma_s}{\tau}W(\xi, s) = \bar{p}'(\xi)\exp(-t_0 s) + \frac{\bar{p}'}{\tau}(\xi)\frac{\exp(-t_0 s)}{s},$$

$$W(\xi, s) = \mathscr{L}[\bar{w}(\xi, t)].$$

$\bar{w}(\xi, 0) = 0$ in order that the final solution is equal to the elastic solution for $t = t_0$. Substituting for $D = a^4\gamma_s/4$ gives

$$\left(1 + \frac{\xi^4\alpha^4}{4}\right)\left(\gamma_s sW(\xi, s) + \frac{\gamma_s}{\tau}W(\xi, s)\right) = \bar{p}'(\xi)\exp(-t_0 s) + \frac{\bar{p}'(\xi)}{\tau}\frac{\exp(-t_0 s)}{s}.$$

Let

$$\tau_\xi = \left(1 + \frac{\xi^4 \alpha^4}{4}\right) \tau,$$

then

$$W(\xi, s) = \frac{\tau}{\gamma_s} \bar{p}'(\xi) \cdot \left(\frac{\exp(-t_0 s)}{\tau s} + \exp(-t_0 s)\right)\left(\frac{1}{s\tau_\xi + 1}\right) \tag{6}$$

and

$$\bar{w}(\xi, t) = \mathscr{L}^{-1}[W(\xi, s)]$$

$$= \frac{\tau}{\gamma_s} \bar{p}'(\xi) \mathscr{L}^{-1}\left[\frac{\exp(-t_0 s)}{\tau s(s\tau_\xi + 1)} + \frac{\exp(-t_0 s)}{(s\tau_\xi + 1)}\right]. \tag{7}$$

Both terms in equation (7) can be inverted by using the convolution property of the Laplace transform and

$$\bar{w}(\xi, t) = \frac{\bar{p}'(\xi)}{\gamma_s} \left[\left(\frac{\tau}{\tau_\xi} - 1\right) \exp(-(t - t_0)/\tau_\xi) + 1\right]. \tag{8}$$

The inverse Hankel transform of (8) is

$$w(r, t) = \int_0^\infty \frac{\bar{p}'(\xi)}{\gamma_s} \left[\left(\frac{\tau}{\tau_\xi} - 1\right) \exp(-t/\tau_\xi) + 1\right] J_0(\xi r) \xi d\xi \tag{9}$$

where we have chosen to apply the surface load at $t_0 = 0$. By setting $t = 0$ and resubstituting for τ_ξ in terms of α and ξ, equation (9) is seen to be equal to the expression for the deformation of an elastic plate. That this is so is physically reasonable since the plate has had no time to relax immediately after the load is applied.

Equation (9) does not specify the spatial form of the surface load function. As for the elastic plate, the most useful result is the Green function. Therefore, choose

$$p(r, t) = p_0 \delta(r - r_0) \cdot H(t - t_0)$$

so that

$$\bar{p}(\xi, t) = \frac{-p_0}{2\pi} \cdot H(t - t_0) = \bar{p}'(\xi) \cdot H(t - t_0). \tag{10}$$

Substituting (10) in (9) gives

$$G(r - r_0, t) = \frac{-p_0}{2\pi\gamma_s} \int_0^\infty \left[\left(\frac{\tau}{\tau_\xi} - 1\right) \exp(-t/\tau_\xi) + 1\right] J_0(\xi r) \xi d\xi \tag{11}$$

where the notation $G(r - r_0, t)$ is used to emphasize that the results are the space-time Heaviside–Green functions for the response of the viscoelastic plate. The terminology is designed to coincide with that used by Peltier (1974).

Before (11) can be integrated, values for the parameters τ, τ_ξ (or equivalently α or D) and γ_s must be chosen. By using the results of Fig. 1 a range of values of τ from 10^5 to 10^7 yr and D from 10^{24} to 10^{26} Nm were decided upon. ρ_m and ρ_s were taken to be 3.4×10^3 and 0 kg m^{-3} respectively, because no sedimentary filling of the depression caused by this point load is required. The equation was integrated for specified values of r from 0 to

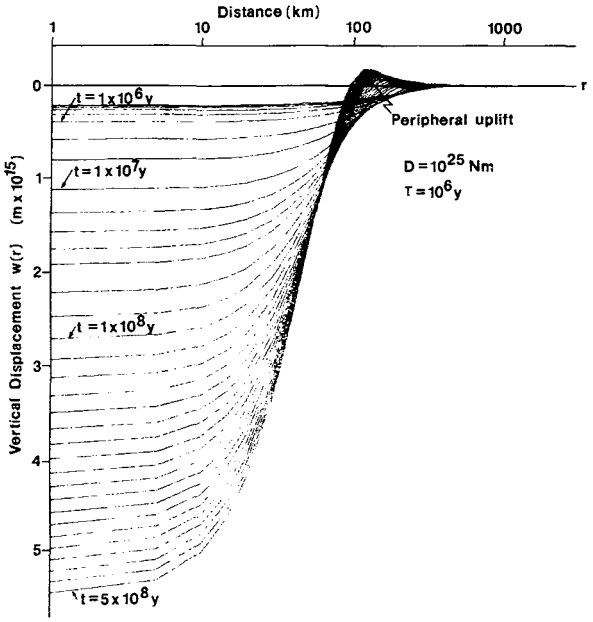

Figure 3. Space-time Heaviside–Green functions for a viscoelastic plate overlying a fluid substratum. The plate properties are $D = 10^{25}$ Nm, $\tau = 10^6$ yr and $\rho_m = 3.4 \times 10^3$ kg m^{-3}. The load is 1 kg. The time-span from 0–500 Myr is not divided into equal intervals. Note: (1) the logarithmic distance scale, (2) the relative amplitudes of the peripheral uplift and central depression and (3) the inward migration of the peripheral bulge with time.

1200 km and for a range of discrete values of t from 0 to 250 Myr. An example of the results is shown in Fig. 3. The integrals were evaluated numerically using Romberg integration (see, e.g. Moursund & Duris 1967) for subintervals of ξ between each of the zeros of $J_0(\xi r)$. The resulting alternating series was summed by Euler contraction. This method proved to be reasonably efficient, requiring integration to approximately the 15th zero of $J_0(\xi r)$ for an accuracy of 0.2 per cent. More terms were needed for values of $r \leqslant 10$ km. However, in this region $G(r - r_0, t)$ is slowly varying for $t \leqslant 200$ Myr and, consequently, only a few values of r were required.

That the asymptotic value of $G(r - r_0, t)$ as $t \to \infty$ is $\delta(r - r_0)$ can be shown by substituting $t = \infty$ in (11) and evaluating the resulting Hankel transforms,

$$\int_0^\infty J_0(\xi r)\xi d\xi \quad \text{for} \quad r > 0$$

and

$$\int_0^\infty \xi d\xi \quad \text{for} \quad r = 0.$$

This is a physically impossible result in that it corresponds to an infinite displacement beneath the point load and not to isostatic equilibrium. Physically meaningful and correct results are given when the surface load is distributed over a finite area. This removes the delta function singularity in load and displacement at the origin. For example, consider the equilibrium of a cylindrical load, radius a, height h and density ρ_l that exerts a surface

pressure $p_0(r) = h\rho_l g$ for $r \leqslant a$. Convolution gives

$$w(r, \infty) = \int_0^\infty G(\mathbf{r} - \mathbf{r}', \infty) p_0(\mathbf{r}) d\mathbf{r}$$

$$= -\frac{1}{\gamma_s} \int_0^\infty \delta(r - r') h\rho g r dr, \qquad r \leqslant a$$

since for an axisymmetric load the θ integration yields 2π. Therefore, $w(r, \infty) = -(h\rho_l g/\gamma_s) = -(h\rho_l/\rho_m)$, $r \leqslant a$ and $w(r, \infty) = 0$ elsewhere. Note; there is no sedimentary infilling by material density ρ_s. This result is the correct isostatic equilibrium position for a cylinder floating in a medium of density ρ_m.

4 Isostatic adjustment under a cylindrical surface load

An interesting application of the theory developed in the previous section is that of isostatic adjustment of cylindrical, or disc, loads on a viscoelastic lithosphere. This problem is important in that it represents an approximation to the isostatic adjustment of volcanic islands, for example the Emperor Hawaiian Island chain. It is also important because it demonstrates that the rate of isostatic adjustment on a viscoelastic lithosphere is largely determined by the spatial extent, or wavelength, of the load. This fact was overlooked by Walcott (1970) and Watts & Cochran (1974), who based their conclusions on a comparison of results for distributed loads on an elastic lithosphere with the Green functions for a two-dimensional load on a viscoelastic lithosphere. They ignored the distribution of the load for the viscoelastic case.

The response $w(r, t)$ to a cylindrical load $p(r)$, radius a, height h and density ρ, at time t, can be determined in one of two ways. The first is to evaluate the convolution

$$w(r, t) = \int_0^\infty \int_0^{2\pi} G(r - r_0, t) p(r) r dr d\theta$$

where

$$p(r) = h\rho g \qquad (0 < r < a)$$

$$= 0 \qquad (r > a).$$

The second is to insert $\bar{p}'(\xi) = h\rho g J_1(\xi a)/\pi\xi a$, the Hankel transform of the cylindrical load (Sneddon 1951, p. 528), into equation (9). The inverse Hankel transform is then evaluated in the manner previously outlined; however, care is required because the zeros of both $J_0(\xi r)$ and $J_1(\xi a)$ must be considered. The first method was found to be the most efficient. Illustrative results are shown in Fig. 4 for cylindrical loads of radii 10 and 100 km on a viscoelastic lithosphere with properties, $D = 10^{25}$ Nm, $\tau = 10^5$ yr, and $\rho_m = 3.4 \times 10^3$ kg m^{-3}. The results show that the 100-km radius load is close to isostatic equilibrium after 200 Myr, whereas adjustment of the 10-km radius load requires a time interval longer than the age of the Earth. Consequently, the simple model explains why short-wavelength topography can remain uncompensated for very long periods of time, whereas long-wavelength features undergo rapid compensation. It also predicts that the degree of compensation will depend on the age of the topography and its spatial wavelength. Banks, Parker & Heustis (1977) have extended Dorman & Lewis's (1970, 1972) and Lewis & Dorman's (1970) work on this problem but have not considered the time dependency.

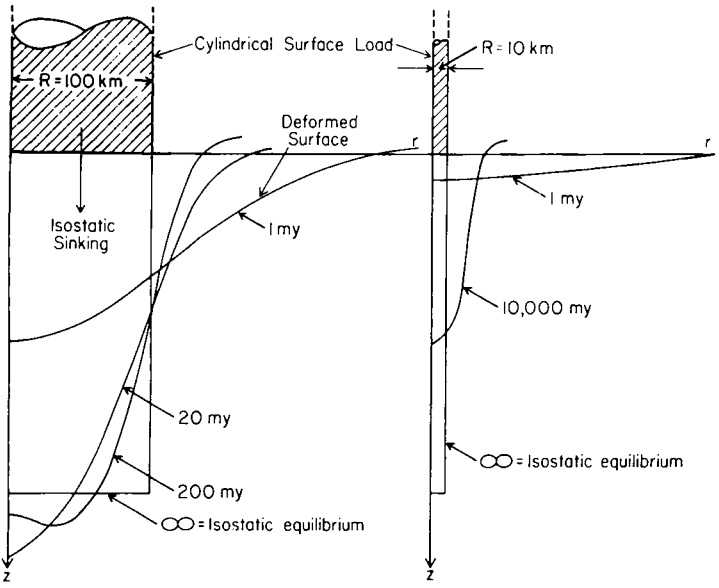

Figure 4. The dynamics of the isostatic adjustment of cylindrical loads on a viscoelastic lithosphere. The properties of the model for both results are: $D = 10^{25}$ Nm, $\tau = 10^5$ yr and $\rho_m = 3.4 \times 10^3$ kg m^{-3}. The figures illustrate the progressive subsidence of cylinders of radii 100 and 10 km into the lithosphere. In particular, $t = \infty$ represents the final position of isostatic equilibrium since the Maxwell body acts as a fluid for very long time-scales. The difference in adjustment rates is solely a function of the differing radii of the cylinders, demonstrating that the rate of isostatic adjustment is a function of the wavelength of the surface load.

The result also partially refutes the criticism of a linear elasticoviscous rheology; that there should be no significant stresses remaining within the lithosphere after a time equal to 2τ. This prediction is true only for long-wavelength stress distributions. For short-wavelength stress the Maxwell model will sustain stresses in a similar manner to a viscoplastic model. To justify a plastic rheology it must be shown that there is a yield stress and, consequently, that isostatic adjustment is a function of the amplitude of the load in addition to its characteristic wavelength.

5 Isostatic adjustment in sedimentary basins

The problem posed and solved in the previous section is directly related to the formation of a sedimentary basin on a viscoelastic lithosphere in that the Heaviside–Green functions are the kernels in the integral equation describing basin formation.

Consider a depression in the Earth's surface, depth $d(\mathbf{r}, t)$. At any point in time, t_0, we need to know how much sediment this depression can accommodate, assuming that there is an instantaneous elastic deformation and that the basin can only be filled to its brim. Implicit in this method of posing the problem is the assumption that there is always sufficient sediment available to fill the basin. Such basins will contain only shallow water facies. Variants on this model based on known, or hypothetical, sedimentary budgets can easily be developed. The total sedimentary load that can instantaneously be accommodated by the basin is

$$L(\mathbf{r}, t_0) = \rho_s g d_L(\mathbf{r}, t_0) + \rho_s g d(\mathbf{r}, t_0) \tag{12}$$

where d_L is the instantaneous deformation caused by the load, and is related to that load by the convolution integral

$$d_L(\mathbf{r}, t_0) = \iint_A G(\mathbf{r} - \mathbf{r}', 0) L(\mathbf{r}', t_0) dA, \tag{13}$$

where A symbolically represents the area over which the integral is evaluated: that is, the basin and its surrounding deformation. Substituting (12) into (13) gives

$$d_L(\mathbf{r}, t_0) = D(\mathbf{r}, t_0) + \rho_s g \iint_A G(\mathbf{r} - \mathbf{r}', 0) d_L(\mathbf{r}', t_0) dA \tag{14}$$

where

$$D(\mathbf{r}, t_0) = \rho_s g \iint_A G(\mathbf{r} - \mathbf{r}', 0) d(\mathbf{r}', t_0) dA.$$

Equation (14) is a Fredholm integral equation of the second kind. The solution, $d_L + d$, is the total instantaneous subsidence of the basin. The integral equation can be solved iteratively using $D(\mathbf{r}, t_0)$ as a first trial for $d_L(\mathbf{r}, t_0)$ in the convolution (Hildebrand 1965, p. 259). Evaluating the integral yields $d_L^{(2)}(\mathbf{r}, t_0)$, the second approximation, which is then returned to the right-hand side and the process repeated. Convergence is rapid and an overall accuracy of 1 per cent is achieved in three or four iterations. The test for convergence is that

$$\iint_A d_L^{(n)}(\mathbf{r}, t_0) dA$$

differs from

$$\iint_A d_L^{(n-1)}(\mathbf{r}, t_0) dA$$

by less than 1 per cent.

The development of the basin with time is considered to occur in discrete steps. If $L(\mathbf{r}, t_0)$ was the instantaneous load accommodated by the basin at t_0, then at a later time, t_1, the basin surface will have subsided by viscoelastic relaxation under the load, and additional sediment can be added. 'Topping up' is easily achieved by re-solving equation (14) with a depression, depth $d(\mathbf{r}, t_1)$, equal to the subsidence of the surface between t_0 and t_1. This subsidence is determined by the difference in deformation, due to the load $L(\mathbf{r}, t_0)$ at t_0 and t_1. That is,

$$d(r, t_1) = \iint_A \Delta G(\mathbf{r} - \mathbf{r}', 0, t_1) L(\mathbf{r}', 0) dA \tag{15}$$

where $\Delta G(\mathbf{r} - \mathbf{r}', 0, t_1)$ is the difference between $G(\mathbf{r} - \mathbf{r}', 0)$ and $G(\mathbf{r} - \mathbf{r}', t_1)$ and t_0 has been taken as 0. Solving equation (14) determines the load, $L(\mathbf{r}, t_1)$, that can be added to the basin and $d_L(r, t_1) + d(r, t_1)$, the total additional deformation of the basin at time t_1.

The development of the basin can be time-stepped forward in this manner. At each time-step the subsidence of the surface of the basin is determined, bearing in mind that equation (15) has to be solved for *each* of the previously accumulated loads using the increment in Green function appropriate for the age of that load. This is required because each load is of a different age and is at a different stage of isostatic adjustment. The model is linear,

therefore the total subsidence, prior to filling, for the timestep t_{n-1} to t_n is

$$d(\mathbf{r}, t_n) = \sum_{i=0}^{n-1} d_i(\mathbf{r}, t_n)$$

where,

$$d_i(\mathbf{r}, t_n) = \iint_A \Delta G(\mathbf{r} - \mathbf{r}', t_{n-1} - t_i, t_n - t_i) L(\mathbf{r}', t_i) dA$$

and $\Delta G(\mathbf{r} - \mathbf{r}', t_{n-1} - t_i, t_n - t_i)$ is the difference in Green functions for a load that was added at t_i, had been undergoing isostatic adjustment for time $t_{n-1} - t_i$ at the last time-step and has been undergoing isostatic adjustment for time $t_n - t_i$ at this time-step. The forward calculation builds a model of the age–depth stratigraphy of the whole basin that can then be compared with observations.

The simple time-stepping described leads to an underestimate of basin subsidence and sediment accumulation because the basin is starved of sediment in the interval between each time-step. A model of a basin that is continuously 'topped up' would, in principle, require an infinitesimal time-step. A finite time-step can, however, be used if a predictor-corrector scheme is used in the time integration. A physical interpretation of this scheme is that calculations of the deformation and load for a given time-step are made. Half the load is then added at the beginning of the time-step rather than waiting until the end. Consequently, the basin is mathematically overfilled for the first half of the time-step and underfilled for the latter half. To a first approximation it remains full throughout the time-step. Higher-order predictor-corrector schemes could be used; however, the first-order scheme was found to be sufficiently accurate, insignificant changes in basin development resulting for quite large variations in the size of the time-step.

6 The initiating mechanism for basin subsidence

The explicit form of the surface depression is a critical component in basin development, for without an initiating mechanism that creates a depression no sediments can accumulate and no basin will develop. The processes involved in initiating subsidence are poorly understood and it is one of the major purposes of this paper to suggest a methodology for recovering the processes, or at least their topographic expression, by deconvolution from the 'known' isostatic adjustment mechanism. The initiating process can be defined as the process describing the development of the basin, were no sediment or water infilling to occur. The observed structure of a sedimentary basin can be modelled by the convolution of the load, filling the initiating depression, with the isostatic response of the lithosphere.

Six possible initiating mechanisms are shown diagrammatically in Fig. 5. The list is by no means exhaustive and the proposed models are archetypes, combinations of two or more may occur in many geotectonic processes. For example, sedimentary basins forming at rifted 'Atlantic type' continental margins probably result from a combination of thermal uplift, erosion and graben formation, followed by rifting, the formation of oceanic crust and cooling (Sleep 1971, for example). With the exception of the thermal uplift-erosion-cooling model, the processes are too poorly understood to be described in a dynamic sense. They can, however, be characterized kinematically by one or two spatial scales ($s_{1,2}$) and a time-scale, τ_i.

Vertical movements associated with phase transitions have been modelled in detail (O'Connell & Wasserburg 1967, 1972 and Mareschal & Gangi 1977a, b, are recent examples).

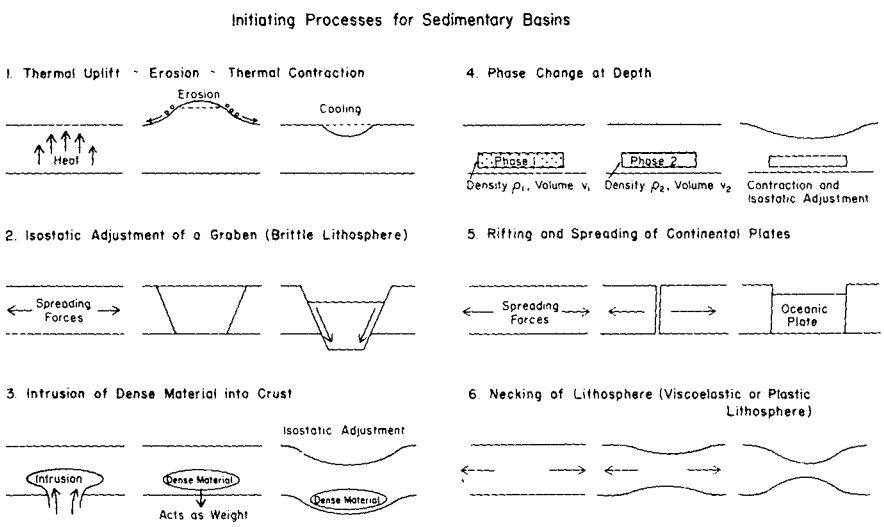

Figure 5. Cartoons representing possible archetypal initiating mechanisms for sedimentary basins.

The results, particularly those of Mareschal & Gangi, can easily be incorporated with the present methodology because they are cast in a Green function form. Such an approach would provide a three-dimensional feedback model for phase transitions within a visco-elastic or elastic lithosphere and consequent sedimentary basin development. It is interesting to note that many sedimentary basins are underlain by regions of anomalously high crustal velocity that may indicate the presence of a more dense, high-velocity phase. Haxby, Turcotte & Bird (1976) invoke the gabbro-eclogite phase transition as the gravitational driving mechanism causing subsidence of the Michigan Basin.

The kinematic form of the initiating mechanism is easily incorporated into the isostatic adjustment calculation described in the previous sections. The function describing the initiating process, $b(\mathbf{r}, t)$, is evaluated for each of the time-steps and the increase in depth, $b(\mathbf{r}, t_n)$, is then added to the increase in depth due to isostatic adjustment, $d(\mathbf{r}, t_n)$, before refilling the basin.

Our poor knowledge of the initiating mechanism is obviously the weak link in the model. Yet, it is in many ways the most interesting. A process of elimination can be invoked for rejecting initiating mechanisms that generate basins that fail to agree with observational evidence. The approach suggested is hardly worse than that used by Sleep & Snell (1976), who chose a gaussian initiating shape, justifying this choice by the fact that most basins have a final cross-sectional shape that is similar to a gaussian curve (Sloss & Scherer 1975). It should be noted that vertical-sided initiating mechanisms can also generate gaussian basins (Beaumont, in preparation). These basins are not in full isostatic equilibrium, yet the dynamic model indicates a rate of isostatic adjustment that is so slow that very little change would be observed over large intervals of time.

7 Examples of basin formation: graben initiated basins

The examples outlined here are not intended to be complete case studies but merely simple illustrative models of the way in which some sedimentary basins, in particular the North Sea, may have developed. The purpose is to identify basin characteristics that are suggestive of

either an elastic or viscoelastic lithosphere and a graben initiating mechanism. Detailed studies of particular basins resulting from a range of initiating mechanisms are the subject of a future paper.

7.1 NUMERICAL CALCULATIONS

The convolutions are evaluated for the central points of a mesh of grid squares. The grid size and number of grid squares are determined by the value of D. For small values of D, α is small and a fine mesh is needed. For large values of $D(\geqslant 10^{25}\,\mathrm{Nm})$ α is large ($\geqslant 186$ km), therefore, the mesh size can be increased to 50 km and yet still provide an accurate picture of the basin. The total grid is taken to include the spatial size of the initiating mechanism, the central depressed region and the peripheral uplifted region surrounding the whole basin (Fig. 6).

Preliminary convolutions were evaluated for each of the Heaviside–Green functions to find the effect of a load uniformly distributed over an area equal to one grid square at the centres of all grid squares. These 'square load response functions' preserve the relationship between the geometry of the grid square and the square load. They correspond to the 'disc factors' used by Peltier & Andrews (1976) and Farrell & Clark (1976) but are more accurate because there is no overlap during superposition of adjacent loads (Fig. 6).

The results of the full calculation are the vertical displacements (subsidence) of the centres of each of the grid squares at the end of each time-step. Relatively few models are required to span a range of flexural rigidities because the results can be scaled. The Heaviside–Green functions $G(\mathbf{r}, t)$ could have been presented in the semi-non-dimensional form $G(\mathbf{r}/\alpha, t)$ since there is a one to one relationship between α and r and therefore a relationship between r/α and $D(=\gamma_s\alpha^4/4)$. Consequently, a change in model D to D' will change r to r' where $r'/r = \alpha'/\alpha = (D'/D)^{1/4}$. The same scaling applies to the complete basin

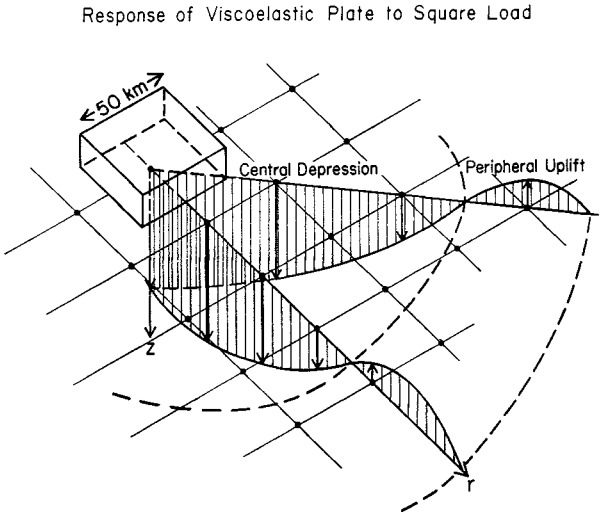

Figure 6. An illustration of a section of the mesh and method of convolution for the numerical calculations. The figure shows the effect of a 50 × 50 km uniform load at neighbouring mesh points. The effect of a distribution of loads is calculated by superposition. The model results in this paper are for a 2-D initiating mechanism, nevertheless, all calculations were made in 3-D as indicated by the figure. Sections through the model results are shown in Figs 9 to 17. Fully 3-D calculations require no changes in the calculation methods.

calculation. For example, a calculation for a 100 x 100 km initiating mechanism on a lithosphere with $D = 10^{25}$ Nm and $\tau = 10^5$ yr can be interpreted as the result for a 178 x 178 km initiating mechanism on a lithosphere with $D = 10^{26}$ Nm and $\tau = 10^5$ yr. The equivalent scaling parameter for the amplitude of deformation is α^2 or $D^{1/2}$.

7.2 THE NORTH SEA

The North Sea sedimentary basin is known to be underlain by a graben system the main arms of which are the north–south trending Viking and Central Graben (Fig. 7). The evolution of the basin has been described in comprehensive reviews by P. Ziegler (1975), Kent (1975) and W. Ziegler (1975). Detailed descriptions of subareas of the basin are to be found in the volume edited by Woodland (1975). In addition, Whiteman *et al.* (1975) have provided a synthesis of the structure of troughs associated with the North Sea Basin.

There is general agreement that the developing North Sea Basin evolved in the following manner. During the Permian, two intracratonic basins occupied the north and south parts of the North Sea separated by the Mid-North Sea–Ringkoebing-Fyn high. The major late Permian deposits in the centres of these basins are the Zechstein halites which locally reach 1 km in thickness. During the Triassic the whole North Sea area underwent a major period

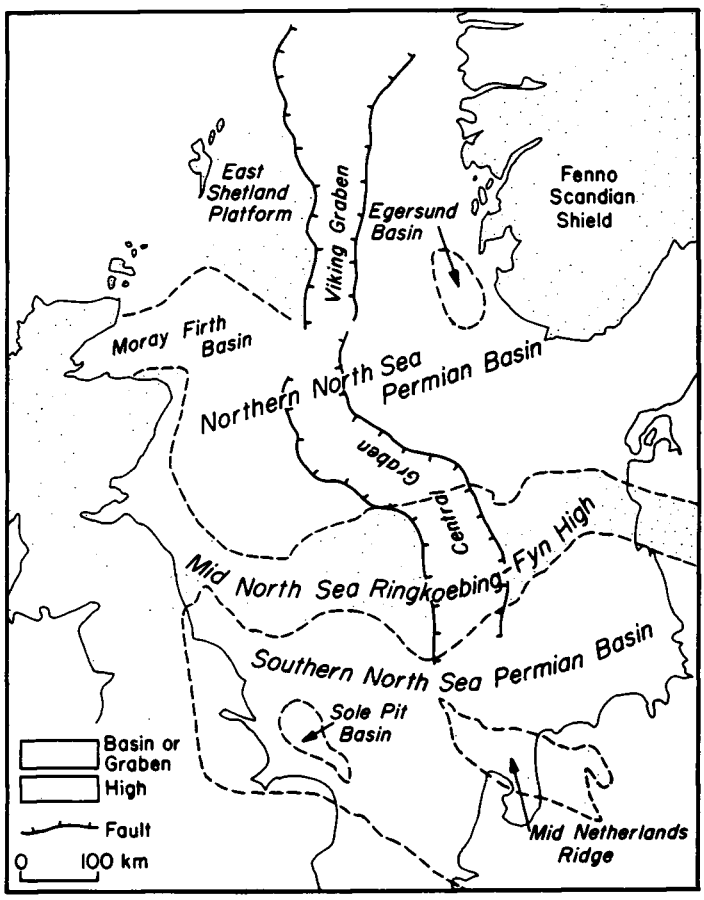

Figure 7. Structural elements of the North Sea Basin.

of taphrogenesis, a precursor to the rifting between North America and Europe. At this time sedimentation was widespread throughout the North Sea indicating that there were no major topographic highs. The Jurassic and Lower Cretaceous, however, were periods of major topographic relief associated with continued rifting and the subsidence of the graben system. During this time only the graben system and subsidiary small basins (e.g. the Sole Pit and Egersund basins, Fig. 7) were significant depocentres. Significant erosion was limited in extent because Triassic deposits are still present in most of the basin and the Zechstein halites are preserved. Those areas where deep erosion has occurred are local centres of distinct Tertiary topographic inversion.

Rifting ceased during the Upper Cretaceous and topographic highs subsided allowing widespread sedimentation over an area averaging 300 km on either side of the basin axis. The late Cretaceous, Tertiary and Quaternary were periods of regional subsidence leading to the development of a saucer-shaped intracratonic basin with axes coincident with the Viking and Central Graben (Fig. 8). This phase, which resulted in a maximum of 3.5 km of Tertiary sedimentary accumulation in the Central Graben, was not fault controlled. Instead, the basin, which decreased in width with time, was apparently under flexural control.

A range of graben-initiated dynamic models which may explain the development of the North Sea Basin are considered. These may be classified as follows:

(1) Flexural Controlled Basins; basins that subside without faulting. The basin, including the initiating mechanism, develops solely by flexure of the lithosphere.

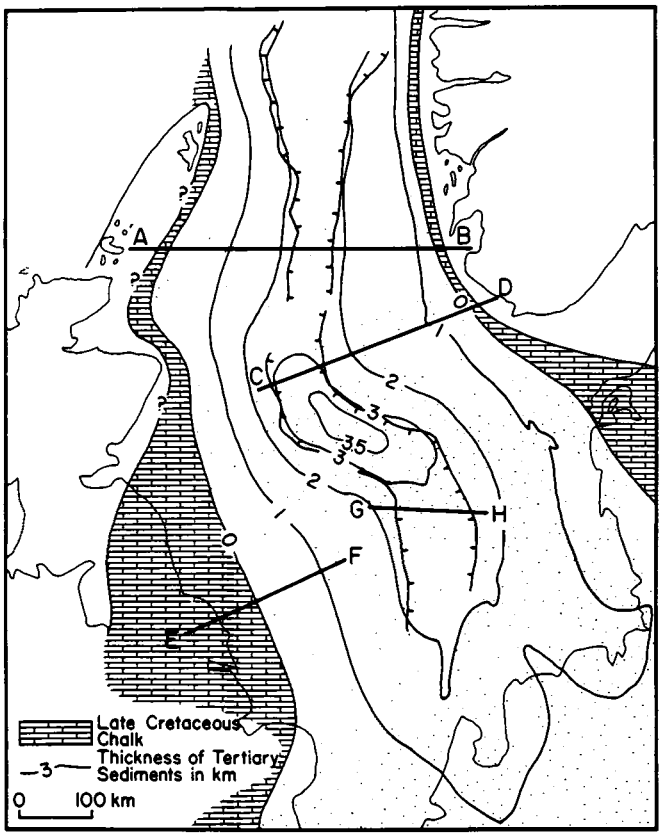

Figure 8. Tertiary isopach map of the North Sea Basin. The lines AB etc. mark the positions of the cross-sections shown in Fig. 18.

(2) Fault Controlled Basins; basins in which the graben initiating mechanism is fault controlled.

(3) Combined Control Basins; basins that were initially fault controlled, but in which the initiating mechanism ceased at some time in the past and, since that time, the basins have been controlled by viscous relaxation of the lithosphere.

Within each of these classes of basin there is a variety of time dependencies for the initiating mechanism and a range of lithospheric properties. Consequently, the range of possible models is large. We concern ourselves with five increasingly sophisticated models that span the range of those possible but do not include every small variation. All calculations were made on either 10×10, 11×11, or 12×12 grids with a mesh size of 50 km and lithospheres having $D = 10^{25}$ Nm.

7.3 MODEL 1: INSTANTANEOUS FAULT-CONTROLLED GRABEN ON AN ELASTIC LITHOSPHERE

This model is the most simple. A vertical-sided infinitely long graben, width 100 km, depth 1 unit is down-faulted instantaneously. It, and the basin formed by the weight of the sediments, are immediately filled with sediment. Uplifted peripheral regions are eroded. The resulting basin (Fig. 9) is ~ 300 km wide if $N = 10^{25}$ Nm and ~ 500 km wide if $N = 10^{26}$ Nm. The asthenosphere is assumed to have a density of 3.4×10^3 kg m^{-3}, that of the sediments 2.4×10^3 kg m^{-3}. Different sediment densities scale the depth of the basin in an approximately linear manner because the major change occurs in γ_s, not α. The results demonstrate that a graben, initially 100 km wide, can give rise to a sedimentary basin of up to 1000 km in width. It should also be noted that the figure represents the final form of the basin. No further development will occur without additional subsidence of the graben due to the initiating mechanism.

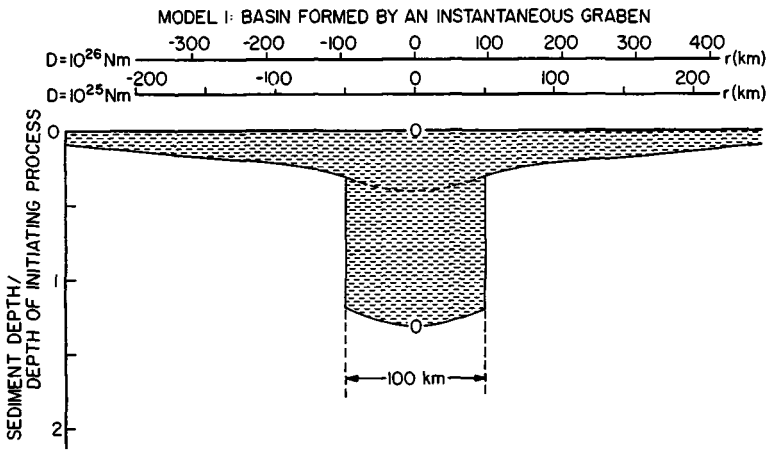

Figure 9. Model 1: Section through the basin formed by an instantaneous 100-km wide graben of depth 1 unit on an elastic lithosphere. Note that the basin is filled instantaneously with sediment and there is no viscous relaxation or change in width of the basin with time. The scales on the abscissa give the size of the basin for $D = 10^{26}$ and 10^{25} Nm. The horizontal scale decreases by a factor of $10^{1/4}$ for an increase of an order of magnitude in D. The corresponding change in the vertical scale is $10^{1/2}$. The vertical scale presented is for $D = 10^{25}$ Nm.

7.4 MODEL 2: INSTANTANEOUS FAULT-CONTROLLED GRABEN ON A VISCOELASTIC LITHOSPHERE

The initiating mechanism is the same as that for model 1 but the basin continues to develop for approximately 20 Myr because the lithosphere ($\tau = 10^5$ yr) relaxes. Development beyond 20 Myr is very slow and almost no additional change occurs over the next 50–100 Myr. The important results (Fig. 10) are that the basin continues to subside after the initiating mechanism has ceased and that the area surrounding the basin is progressively uplifted with time and, in the model, instantaneously eroded. The basin also decreases in width with time because the uplifted area migrates inward toward the basin axis. This is a direct consequence of the form of the space-time Green functions that exhibit a similar peripheral uplifted area that migrates toward the point load (Fig. 3). The resulting basin is characteristic of all those that have a simple initiating mechanism and a viscoelastic lithosphere; the subsiding part of the basin decreases in width with time and peripheral regions are uplifted. Erosion of the uplift gives rise to a regressive horizon at the basin surface that is typical of many basins. Older sediments, and basement predating the formation of the basin, outcrop at the margins; progressively younger sediments outcrop toward the centre. Eustatic sea-level changes or uplift and erosion of the whole basin are normally cited as the reason for this form of structure (Sloss & Scherer 1975). However, these results show that it may be a natural consequence of viscoelastic relaxation. It should also be noted that relaxation associated with a 100-km wide initiating mechanism on a lithosphere with $N = 10^{25}$ Nm, $\tau = 10^5$ yr is substantially complete after 10 Myr. Therefore, basins that have a history of development spanning 100 Myr or more cannot possibly have a geologically instantaneous (< 1 Myr) initiating mechanism. Neither model 1 nor model 2 adequately describes the development of the North Sea Basin where taphrogenic subsidence of the graben system had ceased by the beginning of the Upper Cretaceous (~ 100 Myr BP).

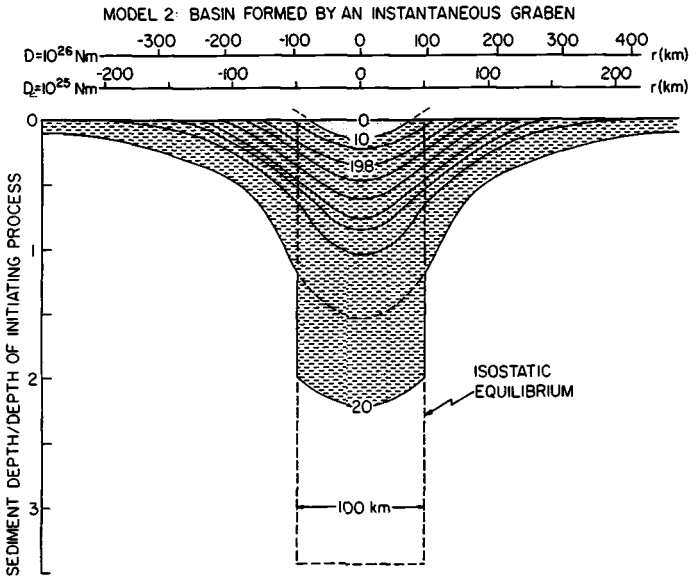

Figure 10. Model 2: Section through the basin formed over a period of 20 Myr by an instantaneous 100-km wide graben of depth 1 unit, on a viscoelastic lithosphere, $\tau = 10^5$ yr. Viscous relaxation produces the increase in depth with time and the decrease in size of the basin. Note, however, that the relaxation is very slow after 2×10^5 yr. The figures 20, 19.8, 10 and 0 refer to the age of the sediments (in millions of years) at those horizons. Horizontal and vertical scalings are the same as those for Fig. 9.

7.5 MODEL 3: EXPONENTIALLY SUBSIDING FAULT-CONTROLLED GRABEN ON A VISCOELASTIC LITHOSPHERE

In this model the initiating mechanism is a vertical-sided 100-km wide graben that subsides exponentially with a time constant of 50 Myr (Fig. 11). Such an initiating mechanism would correspond to thermal control of graben subsidence due to cooling of the lithosphere (Sleep 1971). Forward calculations were carried out for a 100-Myr period and a cross-section of the resulting basin is shown in Fig. 12. The basin is similar to the Upper Cretaceous and later North Sea Basin in that its width decreases with time. The main problem is that faulting continues throughout the development of the basin and therefore even the Tertiary and Quaternary sediments are faulted in the area overlying the graben. The basin does, however, continue to receive sediment for a 100-Myr period and further subsidence is predicted for the future.

7.6 MODEL 4: EXPONENTIALLY SUBSIDING FLEXURE-CONTROLLED BASIN ON A VISCOELASTIC LITHOSPHERE

This model is the same as model 3 except that the development is totally controlled by flexure of the lithosphere.

The results (Fig. 13) show a basin very similar to model 3 except that no faulting has occurred. Monoclinal flexures characteristic of many basins appear on either side of the centre of subsidence. A basin of this type closely resembles the North Sea with the exception that there is no evidence from the stratigraphy of any fault control of the basin.

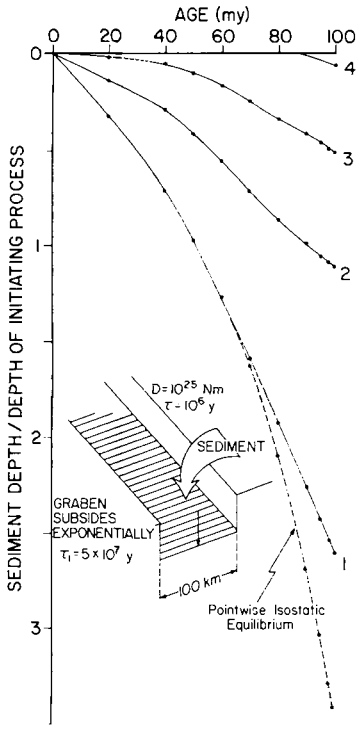

Figure 11. Initiating mechanism and age–depth curves for model basin 3. The curves 1 to 4 represent the age versus depth of the sediments found beneath points 1 to 4 in Fig. 12.

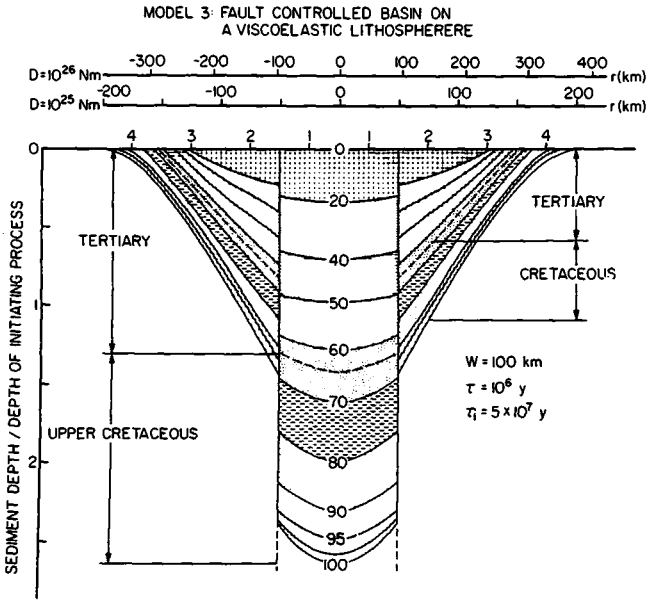

Figure 12. Model 3: Section through the basin formed over a period of 100 Myr by a 100-km wide graben that subsides with a time constant $\tau_i = 5 \times 10^7$ yr on a lithosphere, $\tau = 10^6$ yr. Note that the rate of sediment accumulation does not decrease significantly with time, although the initiating mechanism is slowing at an exponential rate. Note also that the faults bounding the graben extend to the surface because the initiating mechanism remains active throughout the lifetime of the basin. The figures 100 to 0 refer to the age of sediment on those horizons. Horizontal and vertical scalings are the same as those for Fig. 9.

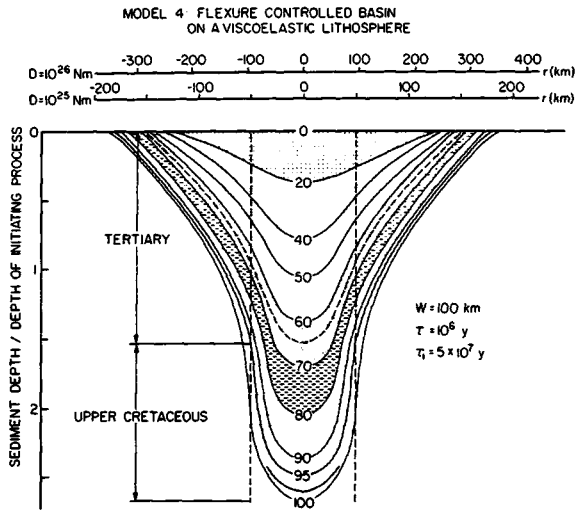

Figure 13. Model 4: Section through the basin formed over a period of 100 Myr by the flexural downwarping of a 100-km wide region that subsides exponentially with a time constant $\tau_i = 5 \times 10^7$ yr on a lithosphere, $\tau = 10^6$ yr. The figures 100 to 0 refer to the age of sediment on those horizons. Horizontal and vertical scalings are the same as those for Fig. 9.

7.7 MODEL 5: EXPONENTIALLY SUBSIDING COMBINED CONTROL GRABEN ON A VISCOELASTIC LITHOSPHERE

In this model, which spans 180 Myr of the history of the North Sea from the Lower Jurassic to the present, a combined initiating mechanism operates. The graben subsides exponentially for the period 180–100 Myr BP (Fig. 14) at which time the initiating mechanism ceases. The Upper Cretaceous and later sediment accumulation (Figs 15, 16 and 17) is solely a result of viscous relaxation of the lithosphere and the approach to pointwise, as opposed to regional, isostatic equilibrium. No subsidence beyond 100 Myr BP would have occurred had the lithosphere been elastic. The model results closely resemble the largest scale of structure of the North Sea (Fig. 18) including the central graben, fault-controlled subsidence prior to the Late Cretaceous, flexure-controlled Tertiary subsidence, and a decrease in basin width with time. No attempt is made to represent secondary faulting or inversions that result from salt or shale diapirism.

The chief attribute of this more complex model is that there is a natural transition from the taphrogenic (180–100 Myr BP) basin to the broad flexural intracratonic basin. This transition occurs at the point in time when the initiating mechanism, graben subsidence, ceases. A similar transition in the subsidence of 'Atlantic type' continental margins has been noted by Kent (1976) and is implicit in discussions by Sheridan (1974, 1976).

The theoretical results are presented in the form of age–depth curves in Figs 11 and 14. These correspond to the age–depth stratigraphy of theoretical wells drilled at points 1–4 in model 3 (Fig. 12) and points 1–3 in model 5 (Fig. 15). An important result is that in the deepest parts of the basin an exponential initiating mechanism results in a nearly linear age–depth relationship (curve 1, Fig. 11). It is only when the initiating mechanism ceases

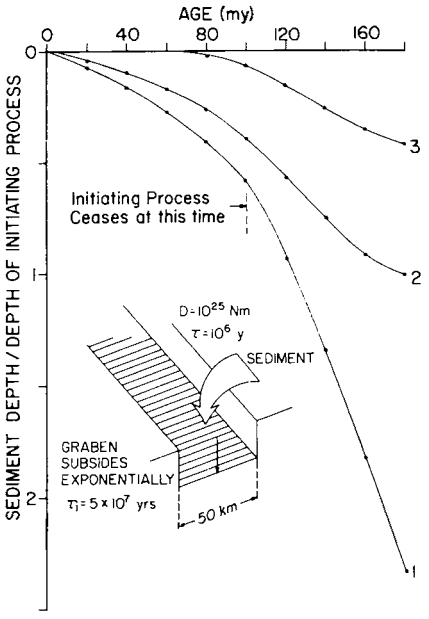

Figure 14. Initiating mechanism and age–depth curves for models 5. A graben that is 50-km wide (Figs 15 and 16) and 100-km wide (Fig. 17) subsides exponentially with a time constant $\tau_i = 5 \times 10^7$ yr for the period 180–100 Myr BP at which time the initiating mechanism ceases. The curves 1 to 3 represent the age versus depth of the sediments found beneath points 1 to 3 in Fig. 15.

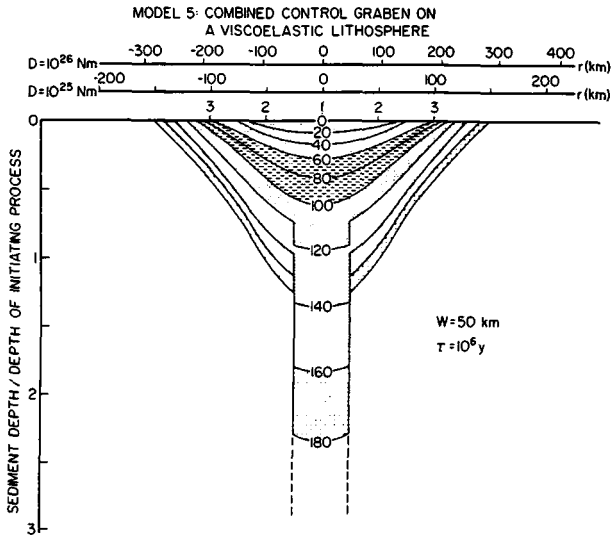

Figure 15. Model 5: section through the basin formed over a period of 180 Myr by a 50-km wide graben that subsides exponentially with a time constant $\tau_i = 5 \times 10^7$yr for the period 180–100 Myr BP and then ceases. The lithosphere has a time constant, $\tau = 10^6$yr. Note that all sediment that accumulates between 100 Myr BP and the present is the result of viscoelastic relaxation during the flexural phase of basin development. Faulting at the boundaries of the graben extends through sediments of ages 180–100 Myr. Horizontal and vertical scalings are the same as those for Fig. 9.

that the characteristic exponential type age–depth curve results (curve 1, Fig. 14). A further interesting result is the sigmoidal nature of the curves for those parts of the basin adjacent to the graben. It should be remembered that these are results for an ideal basin with an infinite sediment budget and no eustatic sea-level changes. Sleep (1976) has shown for a one-dimensional basin, in which local isostatic equilibrium is achieved instantaneously,

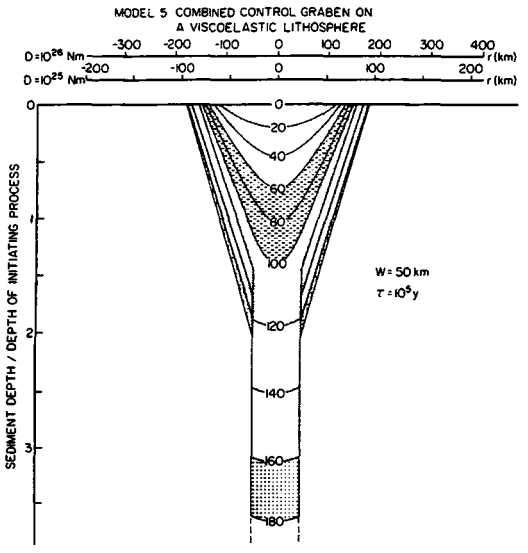

Figure 16. Model 5: section through a basin produced by the same initiating process as that in Fig. 15. However, for this model the lithosphere has a relaxation time constant $\tau = 10^5$yr. Horizontal and vertical scalings are the same as those for Fig. 9.

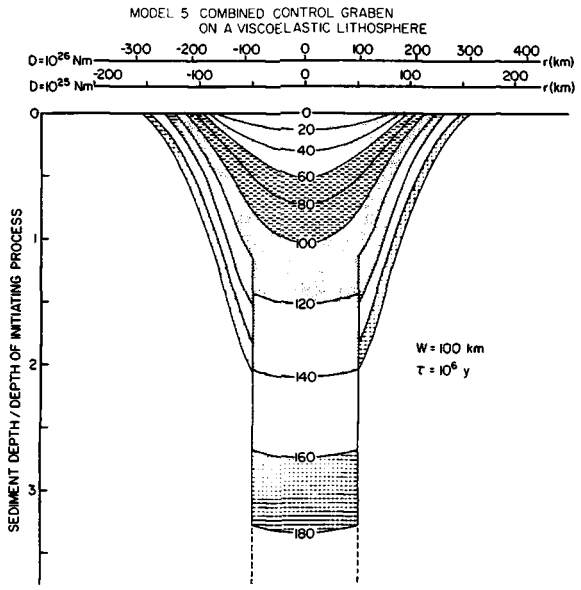

Figure 17. Model 5: section through a basin produced by the same initiating process as that in Fig. 15. However, the graben width is 100 km in this model. Horizontal and vertical scalings are the same as those for Fig. 9.

that sea-level changes cause the age–depth curves to oscillate about those predicted for the ideal basin. Oscillations will also occur for the viscoelastic model, though they will be filtered by the viscous relaxation.

8 Discussion

8.1 A MODEL FOR GRABEN INITIATED BASINS

The kinematics of the transition from taphrogenic to flexural control of subsidence observed in the North Sea can be explained in terms of a simple model based on the horizontal plate motions that create a graben (Fig. 19). Horizontal forces result in failure of the near surface, cool, brittle part of the lithosphere and create major faults dipping at approximately 65° that bound the graben (see Illies 1970 for a discussion of the properties of the Rhine Graben). If spreading occurs across the graben, the graben block will subside because it is no longer in isostatic equilibrium due to its truncated wedge shape (Fig. 19(3)). Sediment accumulation and taphrogenic subsidence will continue until spreading ceases, or until the system achieves isostatic equilibrium (Fig. 19(4)). If spreading across the graben ceases before this equilibrium is reached, the graben block becomes wedged between the adjoining lithospheric blocks, no longer capable of subsiding along the bounding faults. Subsidence continues, however, if the lithosphere is viscoelastic, because relaxation allows continued isostatic adjustment but in a regional sense to form a broad intracratonic basin (Figs 19(5) and 19(6)). This interpretation of model 5 suggests that the transition from taphrogenic to flexural control occurs when spreading across the graben ceases. These ideas are obviously naive and incomplete – thermal uplift, for example, having been ignored. Yet as a working hypothesis they can be developed through quantitative model studies.

Model 5 uses a refinement of the basin transition hypothesis. It is assumed that the graben block's taphrogenic subsidence is sufficiently rapid that it always exerts a downward

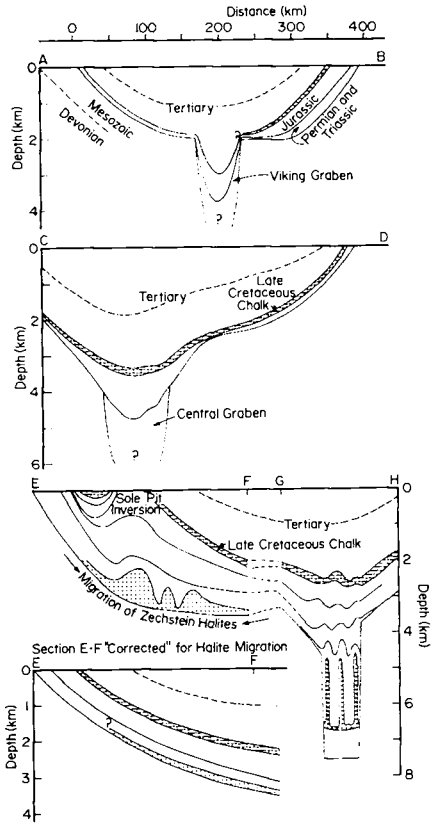

Figure 18. Sections through the North Sea Basin along transects AB, CD, EF and GH of Fig. 8. The largest scale structure is in good agreement with model 5 (Fig. 15). In particular, note that Late Cretaceous and later sediments are not significantly downward block faulted over the Viking and Central Grabens. That the Jurassic sediments adjacent to the graben are thinner than predicted by the model suggests that significant topographic relief in that region during the Jurassic prevented sediment accumulation.

force on the adjoining lithosphere. This downward force results in the simultaneous development of the flexure controlled basin that parallels the graben (Figs 15, 16 and 17).

8.2 VISCOELASTIC OR ELASTIC LITHOSPHERE?

The results presented in this paper do not prove that the rheology of the lithosphere is other than elastic. Any linear system, such as the proposed model, in which the input (the initiating mechanism) and system response (rheology) are both unknowns, cannot be uniquely determined solely from a knowledge of the output (the observed structure of a sedimentary basin). However, certain aspects of the model results that agree with observations would be difficult to explain if the lithosphere were elastic. In point form these are:

(1) The decrease in the size of the basin receiving sediment with age. For an elastic lithosphere this can only occur if the spatial scale of the initiating mechanism decreases with time.

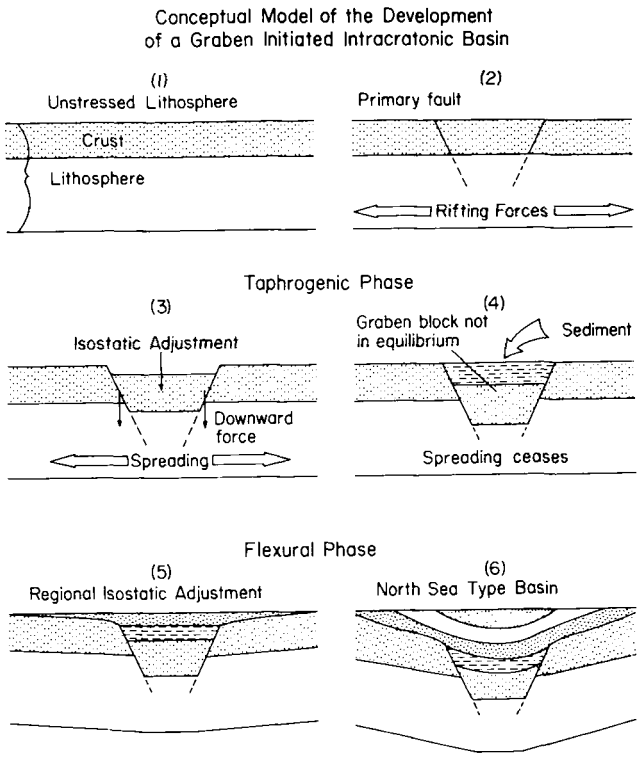

Figure 19. The conceptual model is based on the model results, in particular model 5. It illustrates the proposed model for the development of the North Sea Basin. Note the two main stages of development, taphrogenic and flexural. See text for details.

(2) The form of the erosional surface of the sediment. Only large eustatic sea-level variations would produce such a surface if the lithosphere were elastic.

(3) The natural transition from taphrogenic to flexural control of subsidence. An elastic lithosphere would stop the basin at the end of the taphrogenic phase.

(4) It would be possible to develop a deep sedimentary basin by the proposed mechanisms if the elastic flexural rigidity of the lithosphere were low, $\sim 10^{21}$ Nm. However, for such a low flexural rigidity the basin would be narrow (or small). The combination of final depth and initial width is a clear indication that relaxation in some sense occurs within the lithosphere.

The preferred model for the North Sea Basin has $D \sim 5 \times 10^{25}$ Nm and $\tau \sim 10^6$ yr. For $\tau = 10^5$ yr, the value advocated by Walcott (1970), the model results (Fig. 17) predict a basin that is much too narrow unless $D \gg 10^{26}$ Nm. If the seismic value of D is an upper bound, $\tau \geqslant 5 \times 10^5$ yr. These results are in general agreement with those of a recent study of isostasy on a continental scale by McNutt & Parker (1977). Their results suggest a lower effective flexural rigidity for the Australian lithosphere than that for the United States. The interpretation is that because topography in Australia is on average older than that in the United States, isostatic adjustment and viscoelastic relaxation have proceeded further. Their estimate of $\tau \sim 10^7$ yr is not incompatible with the 10^6 yr chosen as a result of this study. Both estimates are crude, but suggest promising directions for further research.

9 Conclusions

The main purpose of this paper has been to develop a systematic approach to linear modelling of sedimentary basin development. When treated as a linear system, basin formation can be partitioned into input (the initiating mechanism), for which six archetypes are proposed, and system response (isostatic adjustment), governed by the rheology of the lithosphere. Basin subsidence and sediment accumulation are determined by the convolution of initiating mechanism and isostatic adjustment.

The theory of isostatic adjustment on elastic and viscoelastic lithospheres was developed in terms of space-time Green functions for simple thin plate models of the lithosphere. Extension to more complex, but linear, earth models is in principle straightforward. It is shown that the rate of isostatic adjustment on a viscoelastic lithosphere is strongly dependent on the spatial scale of the surface load.

Sediment accumulation within a basin is governed by the sediment budget and the rate at which subsidence occurs. Subsidence rates are given by the solution of an integral equation with the isostatic space-time Green functions as kernel.

The predictions of a model where the initiating mechanism is the formation of a graben, which is subsequently filled with sediment, are compared with the largest scale structure of the North Sea Basin. A model in which the initiating mechanism operated from 180–100 Myr BP on a lithosphere, with flexural rigidity $D = 5 \times 10^{25}$ Nm and viscous time constant $\tau = 10^6$ yr is in good agreement with the largest scale features of the North Sea Basin. The results, however, are preliminary and only intended to illustrate the technique. They are not a definitive study of the origin of the North Sea Basin. This must await the conclusions of basin models with other initiating mechanisms. The results are, however, encouraging because they demonstrate that a basin, like the North Sea Basin, can result from the natural evolution of sedimentary loads that accumulate in a graben if the lithosphere is viscoelastic.

Acknowledgments

The author would like to thank Jack Sweeney of the Earth Physics Branch for interesting him in the sedimentary basin problem. Chris Garrett provided insight on some aspects of the mathematics. Randell Stephenson and Garry Quinlan critically read an earlier version of the manuscript. This work was supported by the National Research Council of Canada and the Gravity and Geodynamics Division of the Earth Physics Branch, Energy Mines and Resources, Ottawa.

References

Banks, R. J., Parker, R. L. & Heustis, S. P., 1977. Isostatic compensation on a continental scale: local versus regional mechanisms, *Geophys. J. R. astr. Soc.*, submitted.

Cathles, L. M., 1975. *The viscosity of the Earth's mantle*, Princeton University Press, New Jersey.

Dorman, L. M. & Lewis, B. T. R., 1970. Experimental isostasy, 1, theory of the determination of the Earth's isostatic response to a concentrated load, *J. geophys. Res.*, **75**, 3357–3365.

Dorman, L. M. & Lewis, B. T. R., 1972. Experimental isostasy, 3, inversion and isostatic changes, *J. geophys. Res.*, 77, 3068–3077.

Farrell, W. E. & Clark, J. A., 1976. On postglacial sea level, *Geophys. J. R. astr. Soc.*, **46**, 647–667.

Gunn, R., 1943. A quantitative evaluation of the influence of the lithosphere on the anomalies of gravity, *J. Franklin Inst.*, **236**, 373–396.

Hanks, T. C., 1971. The Kuril Trench–Hokkaido Rise system: large shallow earthquakes and simple models of deformation, *Geophys. J. R. astr. Soc.*, **23**, 173–189.

Haxby, W. F., Turcotte, D. L. & Bird, J. M., 1976. Thermal and mechanical evolution of the Michigan Basin, *Tectonophys.*, **36**, 57–75.

Hertz, H., 1884. On the equilibrium of floating elastic plates, *Wiedemann's Ann.*, **22**, 449–455.
Hildebrand, F. B., 1965. *Methods of applied mathematics*, Prentice-Hall, New Jersey.
Illies, J. H., 1970. Graben tectonics related to crust–mantle interaction, in *Graben problems*, pp. 4–26, eds, Illies, J. H. & Mueller, St.
Jeffreys, H., 1959. *The Earth*, 4th edn, Cambridge University Press, London.
Kent, P. E., 1975. Review of North Sea Basin development, *J. Geol. Soc. London*, **131**, 435–468.
Kent, P. E., 1976. Major synchronous events in continental shelves, *Tectonophys.*, **36**, 87–91.
Lewis, B. T. R. & Dorman, L. M., 1970. Experimental isostasy, 2, an isostatic model of the United States derived from gravity and topographic data, *J. geophys. Res.*, **75**, 3367–3386.
Mareschal, J. C. & Gangi, A. F., 1977a. A linear approximation to the solution of a one-dimensional Stefan problem and its geophysical implications, *Geophys. J. R. astr. Soc.*, **49**, 443–458.
Mareschal, J. C. & Gangi, A. F., 1977b. Equilibrium position of a phase boundary under horizontally varying surface loads, *Geophys. J. R. astr. Soc.*, **49**, 757–772.
McNutt, M. K. & Parker, R. L., 1977. Isostasy in Australia and the evolution of the compensation mechanism, *Science*, in press.
Moursund, D. G. & Duris, C. S., 1967. *Elementary theory and application of numerical analysis*, McGraw-Hill, New York.
Murrell, S. A. F., 1976. Rheology of the lithosphere – experimental indications, *Tectonophys.*, **36**, 5–24.
Nadai, A., 1963. *Theory of flow and fracture of solids*, **2**, McGraw-Hill, New York.
Oberhettinger, F., 1972. *Tables of Bessel transforms*, Springer-Verlag, New York.
O'Connell, R. J. & Wasserburg, G. J., 1967. Dynamics of the motion of a phase change boundary to changes in pressure, *Rev. Geophys. Space Phys.*, **5**, 329–410.
O'Connell, R. J. & Wasserburg, G. J., 1972. Dynamics of submergence and uplift of a sedimentary basin underlain by a phase-change boundary, *Rev. Geophys. Space Phys.*, **10**, 335–368.
Peltier, W. R., 1974. The impulse response of a Maxwell earth, *Rev. Geophys. Space Phys.*, **12**, 649–669.
Peltier, W. R. & Andrews, J. T., 1976. Glacial-isostatic adjustment – I. The forward problem, *Geophys. J. R. astr. Soc.*, **46**, 605–646.
Sheridan, R. E., 1974. Conceptual model for the block fault origin of the North American Atlantic continental margin geosyncline, *Geology*, **2**, 465–468.
Sheridan, R. E., 1976. Sedimentary basins of the Atlantic margin of North America, *Tectonophys.*, **36**, 113–132.
Sleep, N. H., 1971. Thermal effects of the formation of Atlantic continental margins by continental break-up, *Geophys. J. R. astr. Soc.*, **24**, 325–350.
Sleep, N. H. & Snell, N. S., 1976. Thermal contraction and flexure of mid-continent and Atlantic marginal basins, *Geophys. J. R. astr. Soc.*, **45**, 125–154.
Sleep, N. H., 1976. Platform subsidence mechanisms and 'eustatic' sea-level changes, *Tectonophys.*, **36**, 45–56.
Sloss, L. L. & Scherer, W., 1975. Geometry of sedimentary basins: applications to Devonian of North America and Europe, *Geol. Soc. Am. Mem.*, **142**, 71–88.
Sneddon, I. N., 1951. *Fourier transforms*, McGraw-Hill, New York.
Turcotte, D. L., McAdoo, D. C. & Caldwell, J. G., 1978. An elastic-perfectly plastic analysis of the bending of the lithosphere at a trench, *Tectonophys.*, **47**, 193–205.
Walcott, R. I., 1970. Flexural rigidity, thickness and viscosity of the lithosphere, *J. geophys. Res.*, **75**, 3941–3954.
Walcott, R. I., 1973. Structure of the Earth from glacioisostatic rebound, *Ann. Rev. Earth planet. Sci.*, **1**, 15–37.
Watts, A. B. & Cochran, J. R., 1974. Gravity anomalies and flexure of the lithosphere along the Hawaiian–Emperor seamount chain, *Geophys. J. R. astr. Soc.*, **38**, 119–141.
Watts, A. B., Cochran, J. R. & Selzer, G., 1975. Gravity anomalies and flexure of the lithosphere: a three-dimensional study of the Great Meteor Seamount, Northeast Atlantic, *J. geophys. Res.*, **80**, 1391–1398.
Whiteman, A., Naylor, D., Pegrum, R. & Rees, G., 1975. North Sea troughs and plate tectonics, *Tectonophys.*, **26**, 39–54.
Woodland, A. W. (ed.), 1975. *Petroleum and the continental shelf of north-west Europe*, **1**, John Wiley and Sons, New York.
Ziegler, P. A., 1975. Geological evolution of North Sea and its tectonic framework, *Am. Ass. petrol. Geol. Bull.*, **59**, 1073–1097.
Ziegler, W. H., 1975. Outline of the geological history of the North Sea, in *Petroleum and the continental shelf of north-west Europe*, ed. Woodland, A., **1**, pp. 165–190.